Redox Biology 40 (2021) 101849

Contents lists available at ScienceDirect

Redox Biology

journal homepage: www.elsevier.com/locate/redox

Trem2 mediated Syk-dependent ROS amplification is essential for osteoclastogenesis in periodontitis microenvironment

Yuteng Weng, Haicheng Wang, Lin Li, Yanhuizhi Feng, Shuyu Xu, Zuolin Wang *

Department of Implantology, School and Hospital of Stomatology, Tongji University, Shanghai Engineering Research Center of Tooth Restoration and Regeneration, Shanghai, China

ARTICLE INFO

Keywords:
Triggering receptor expressed on myeloid cells 2 (Trem2)
Reactive oxygen species (ROS)
Osteoclastogenesis
Periodontitis
Nuclear Factor-κB (NF-κB)

ABSTRACT

Periodontitis is the sixth most prevalent diseases around the globe, which is closely related to many systemic diseases and affects general health. As the leading cause of tooth loss, periodontitis is characterized by irreversible alveolar bone loss and activated osteoclastogenic process, which might be closely related to the activated intracellular reactive oxygen species (ROS) in osteoclasts. Here, we demonstrated triggering receptor expressed on myeloid cells 2 (Trem2) as a key regulator of osteoclastogenesis with the regulation of intracellular ROS signals in periodontitis. In the present study, the expression of *Trem2* was significantly upregulated in human alveolar bones diagnosed with chronic periodontitis, as assessed by RNA-seq. In the mice model of periodontitis, the alveolar bone resorption was impeded in the presence of the conditional knockout of *Trem2* in osteoclasts. Furthermore, we identified Trem2/DAP12/Syk-dependent cascade as a vital intracellular signaling for the amplification of reactive oxygen species (ROS) signals in osteoclastogenesis, while the accumulation of soluble $A\beta_{42}$ oligomers (Aβo) in periodontitis microenvironment further strengthened the signals and enhanced osteoclastogenesis through direct interactions with Trem2. Collectively, Trem2 mediated ROS signal amplification cascade was crucial in the process of osteoclastogenesis in periodontitis, suggesting the potential of Trem2 as a target for the prevention and treatment of bone destruction in periodontitis.

1. Introduction

Periodontitis is a common disease characterized by continuous activation of osteoclasts and irreversible alveolar bone loss [1]. As the sixth most prevalent disease worldwide, the progression of periodontitis had been proved to be associated with a variety of systemic diseases [2–5]. In addition, the periodontitis-induced tooth loss severely affected the patients' overall health, including the digestion and cognition, and shortened life expectancy [6,7]. Therefore, searching for the functional regulator and elucidating the mechanisms of osteoclastogenesis in periodontitis microenvironment is greatly significant in clarifying the pathogenesis and providing treatment strategies for the disease.

Osteoclastogenesis was mediated by the stimulation of nuclear factor receptor activator κB ligand (RANKL) and macrophage colony-stimulating factor (M-CSF), while nuclear factor-κB (NF-κB), nuclear factor activated T-cells 1 (NFATc1), and c-Fos served as the leading downstream regulators. This process was finely regulated by RANK and costimulatory signals, both of which are indispensable [8]. The key costimulatory signal was mediated by the immune receptor, stimulated by the immune receptor tyrosine-based activation motif (ITAM) and characterized by the lack of extracellular ligand-binding domain. The motif-mediated intracellular signal transduction was effectuated via the recruitment and phosphorylation of Syk tyrosine kinase [9].

Triggering receptor expressed on myeloid cells 2 (Trem2) is a superimmunoglobulin receptor that receives costimulatory signals [10]. The co-receptor system composed of Trem2 and ITAM-adaptor protein DNAX activation protein 12 kDa (DAP12) plays an essential role in osteoclastogenesis and cognitive maintenance [11]. In vitro, the dysfunction of either Trem2 or DAP12 leads to significantly impaired osteoclastogenesis. In vivo, the functional deficiency of Trem2 or DAP12 results in Nasu-Hakola disease, a recessive hereditary disease characterized by rapidly progressive cognitive impairment and bone involvement symptoms, such as large bone cyst, osteopenia, and early-onset degenerative arthritis [12]. However, the craniomaxillofacial bone was not involved in the pathological changes of the disease. Therefore, whether Trem2 affected the biological behavior of osteoclasts in periodontitis microenvironment and physiological remodeling is yet to be elucidated.

* Corresponding author.
E-mail address: zuolin@tongji.edu.cn (Z. Wang).

https://doi.org/10.1016/j.redox.2020.101849
Received 15 September 2020; Received in revised form 4 December 2020; Accepted 24 December 2020
Available online 28 December 2020

As the secondary signal of osteoclasts, reactive oxygen species (ROS) was produced in RANKL-induced osteoclastogenesis. The level of intracellular ROS indicated the differentiation outcome of osteoclasts [13]. In macrophages and microglia, Trem2 mediates endocytosis by interacting with various ligands and upregulating the ROS level, suggesting the putative role of Trem2 in regulating the intracellular ROS level [14,15]. Presently, the RANKL-RANK-TRAF6-Rac1-Nox signal axis was considered to be the main cascade in regulating the ROS level during osteoclastogenesis [13]. Therefore, whether Trem2 could regulate the differentiation outcome of osteoclasts by monitoring the intracellular ROS production needs further investigation.

Beta-amyloid (Aβ) consists of peptides composed of 38–43 amino acids and is obtained by hydrolysis of amyloid protein precursor (APP). Three forms of Aβ are known to occur in vivo: monomer, oligomer, and fiber. The deposition of Aβ in the brain area was considered as the main cause of cognitive degradation in Alzheimer's disease (AD) [16], which could be induced by the colonization of the pathogen of periodontitis, *Porphyromonas gingivalis* (*P.g*) [2]. Physiologically, the Trem2-mediated endocytosis of Aβ alleviates the cognitive decline [17], proving the existence of a specific interaction pattern between Aβ and Trem2 in the brain region. However, whether similar interactions occur with specific biological functions between Aβ and Trem2 in the periodontitis microenvironment is yet unknown.

In this study, we demonstrated that Trem2 plays a vital role in the

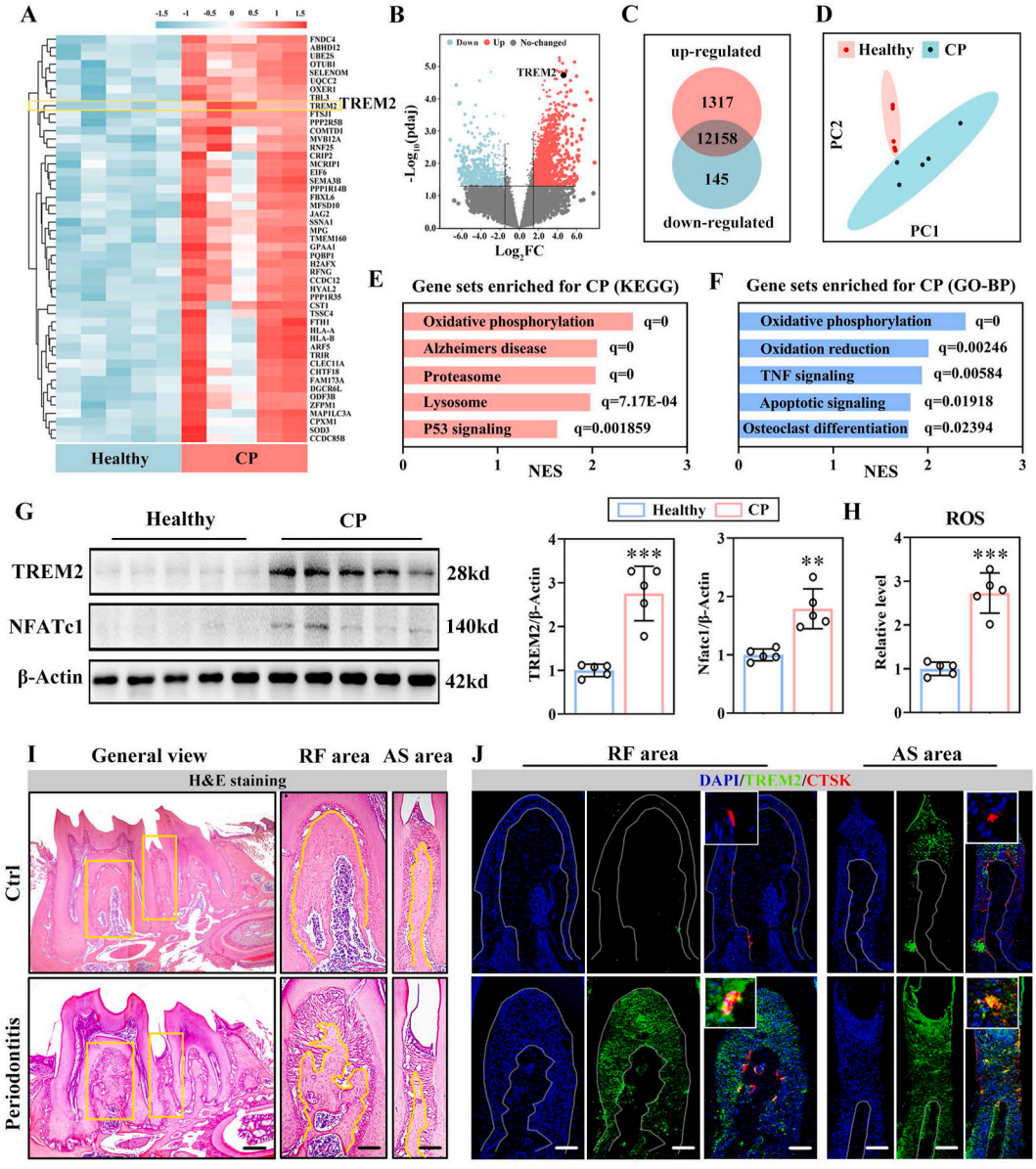

Fig. 1. Trem2 was enriched in pathological alveolar bone remodeling in periodontitis. **(A)** The heat map of the top 50 enriched genes in the alveolar bone samples of patients diagnosed with chronic periodontitis as compared to those of healthy donors based ($n = 5$). **(B)** Volcano plots of the differentially expressed genes. **(C)** Venn diagrams of the number of differentially expressed genes. **(D)** PCA of the samples. **(E)** GSEA using the KEGG database. **(F)** GSEA with database of GO-BP. **(G)** WB analysis of the expression levels of TREM2 and NFATc1 in the healthy and CP group (left). The relative expression levels normalized against the healthy controls (set at 1, right, $n = 5$). **(H)** The ROS level of the healthy and periodontitis alveolar bone samples by DCFH-DA, with the level of healthy group set at 1 ($n = 5$). **(I)** H&E staining images of mandibles from periodontitis and control mice, with the general view (left) and enlarged views of RF (center) and AS (right). The zoomed area and the outline of alveolar bones indicated by the yellow box (left) and line (right), respectively ($n = 4$). Scale bar, 250 μm (left), 100 μm (right). **(J)** DAPI, anti-TREM2, and anti-CTSK mIF staining images of RF (left) and AS (right) areas from control and periodontitis mice. Scale bar, 100 μm ($n = 4$). Values present mean ± SEM: N.S., not significant; $^{*}P < 0.05$, $^{**}P < 0.01$, and $^{***}P < 0.001$ by unpaired two-tailed Student's t-test.

regulation of osteoclastogenesis. In the periodontitis microenvironment, Trem2 amplified the intracellular ROS level and mediated the differentiation of osteoclasts through a Syk-dependent signaling cascade. The deposition of Aβ oligomers in the periodontal area further promoted this pathological process in a Trem2-dependent manner. Taken together, Trem2 could be a novel target for the prevention and treatment of alveolar bone resorption in periodontitis.

2. Results

2.1. Trem2 was enriched in pathological alveolar bone remodeling in periodontitis

To identify the functional genes in bone remodeling of chronic periodontitis (CP), high-throughput RNA sequencing (RNA-seq) of alveolar bone samples from 5 healthy donors and patients diagnosed with CP was performed. The heatmap displayed the top 50 upregulated genes in the CP group in comparison to the healthy group (Fig. 1A, read count >10 was set as the quantification threshold). The differential expressed genes (DEGs) were displayed intuitively by the volcano map with the threshold of $\log_2$FC>1.5 and adjusted P-value <0.05, indicating TREM2 to be a significantly increased differentially expressed gene in the pathological alveolar bone remodeling (Fig. 1B). A total of 1462 genes, including 1317 upregulated genes and 145 downregulated genes, exhibited different expression patterns during bone remodeling in the periodontitis environment (Fig. 1C), and the principal component analysis (PCA) showed the grouped samples with distinct clustering characteristics (Fig. 1D). The gene set enrichment analysis (GSEA) indicated that the gene expression patterns in the CP group were mainly distributed in the signals such as oxidative phosphorylation (according

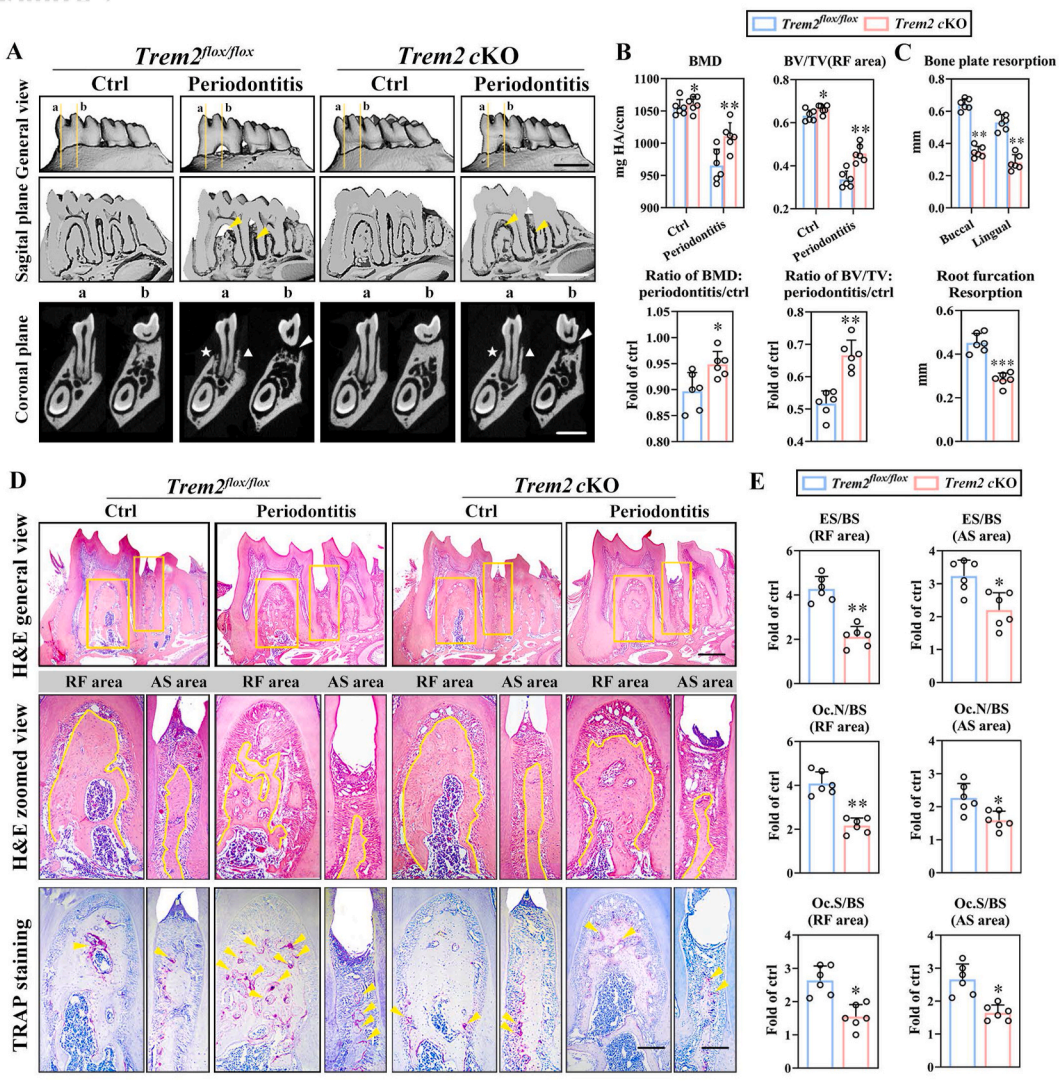

Fig. 2. Osteoclast-specific knockout of Trem2 reduces alveolar bone resorption in periodontitis. (A) Representative micro-CT images of mice mandibles with periodontitis in a general view (top), sagittal view (middle), and coronal view (bottom). Resorptions in the areas of RF and AS observed in the sagittal plane, indicated by the yellow arrows (middle). The coronal planes, cut in the center of the mesial root of the first molar (M1) and RF, respectively, shown as the line a and b (top), with the white triangles, stars, and arrows (bottom) indicating the buccal, lingual bone plates, and RF area, respectively. Scale bar, 1 mm ($n = 6$). **(B)** Bone histomorphometric analysis of BMD, BV/TV (top) in the alveolar bones from *Trem2*$^{flox/flox}$ and *Trem2*-cKO mice and calculated ratio of periodontitis to controls of the two groups (bottom) ($n = 6$). **(C)** Measurements of bone resorption levels in the bone plates of buccal and lingual sides and in the area of RF ($n = 6$). **(D)** H&E staining (top and middle) and TRAP staining (bottom) of mandibles from periodontitis and control mice, with the general view (top) and enlarged views of RF and AS (middle, bottom) indicated by the yellow square (top). The depicted outline of alveolar bones by yellow line (middle) (n = 6). Scale bar, 250 μm (top), 100 μm (middle and bottom). **(E)** Bone resorption parameters of alveolar bones in areas of RF and AS subjected to periodontitis. Values from periodontitis bones were normalized against data from their contralateral controls, which were set at 1 ($n = 6$). Values present mean ± SEM: N.S., not significant; *$P < 0.05$, **$P < 0.01$, and ***$P < 0.001$ by unpaired two-tailed Student's t-test.

to the KEGG database, Fig. 1E), and the functional enrichment was mainly concentrated in processes, such as oxidative phosphorylation and osteoclast differentiation (according to the GO-BP database, Fig. 1F). Thus, the enhanced oxidative stress, inflammation, and strengthened osteoclastogenesis were the characteristic biological changes in alveolar bone remodeling in chronic periodontitis. The increased levels of TREM2 and NFATc1 proteins, combined with the significantly improved ROS level, confirmed the above changes (Fig. 1G, H), indicating a correlation between the expression pattern of TREM2 and the osteoclastogenesis and ROS level in periodontitis microenvironment.

To ensure the distribution of Trem2 in periodontal tissues, we established a periodontitis mouse model and observed significant alveolar bone resorption in the areas of root furcation (RF) and alveolar septum (AS) (Fig. 1I). In the periodontitis microenvironment, the notably improved Trem2 was mainly distributed in the mature osteoclasts and periodontal ligament cells, suggesting that Trem2 might be closely related to the activity of osteoclasts in alveolar bone remodeling

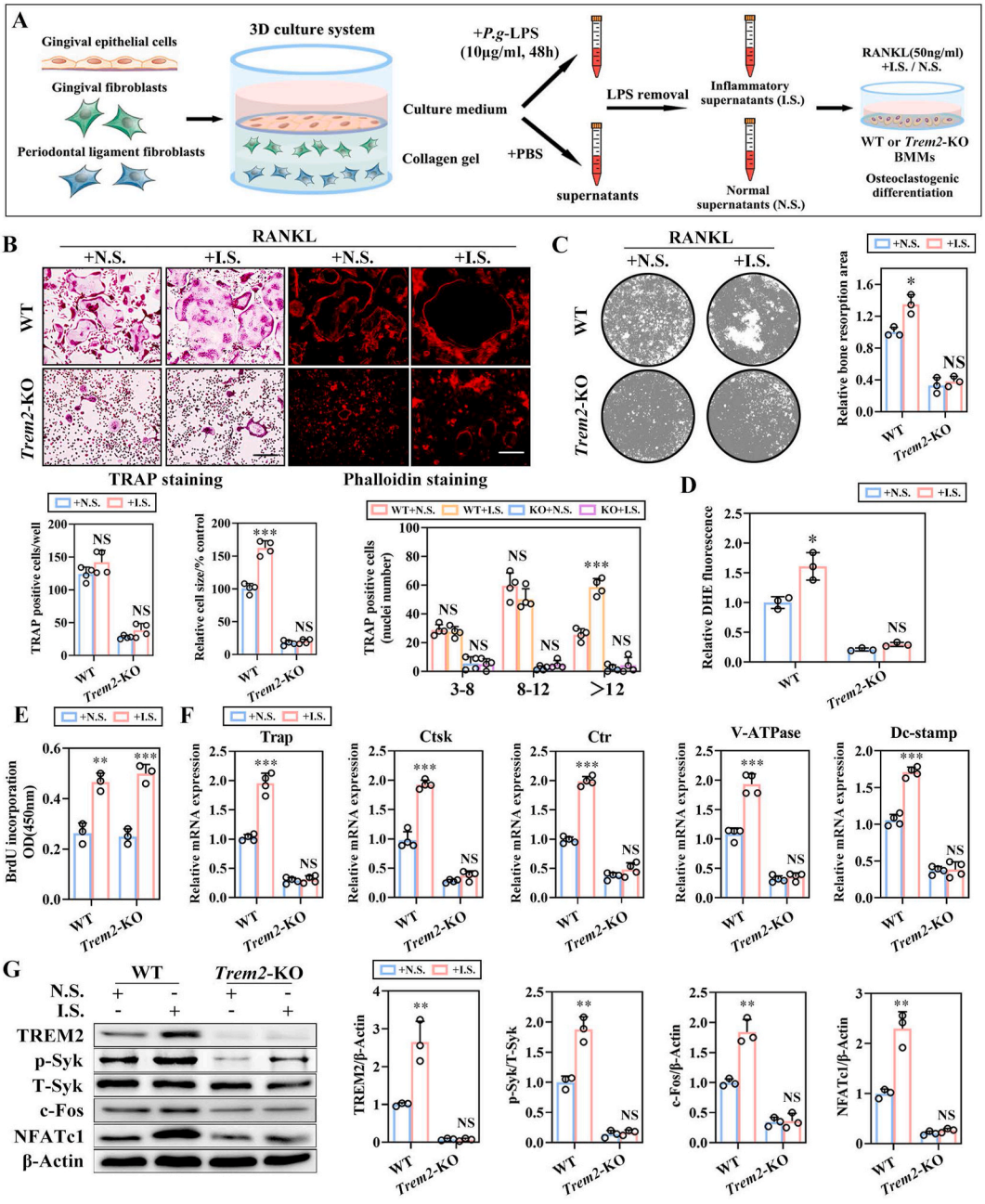

Fig. 3. Trem2 mediates osteoclastogenesis in the in vitro simulation of periodontitis microenvironment by 3D co-culture system. **(A)** The pattern graph of the experimental workflow of the simulation of periodontitis microenvironment in vitro based on 3D co-culture system. **(B)** Representative images for $TRAP^+$ osteoclasts and actin belt formation by TRAP and rhodamine-phalloidin staining in WT or *Trem2*-KO OCs by the combined applications of RANKL and normal supernatants (NS) or inflammatory supernatants (IS), respectively. Scale bar, 100 μm. The cell number, nuclei number, and relative cell size of the $TRAP^+$ OCs were quantified (bottom) ($n = 4$). **(C)** Representative images for bone resorption (left) and quantification of resorption areas (right) by OCs ($n = 3$). **(D)** The ROS levels of BMMs were measured by DHE ($n = 3$). **(E)** The measurements of proliferation by BrdU incorporation in WT or *Trem2*-KO BMMs for 3 days ($n = 3$). **(F)** The mRNA expression of *Trap*, *Ctsk*, *Ctr*, *V-ATPase,* and *Dc-stamp* in WT or *Trem2*-KO OCs ($n = 4$). **(G)** The expression of TREM2, c-Fos, and NFATc1, along with the phosphorylation of Syk by WB (left) with quantitative analysis (right) ($n = 3$). Values present mean ± SEM: N.S., not significant; $^*P < 0.05$, $^{**}P < 0.01$, and $^{***}P < 0.001$ by unpaired two-tailed Student's t-test.

in periodontitis microenvironment (Fig. 1J).

2.2. Osteoclast-specific knockout of Trem2 reduces alveolar bone resorption in periodontitis

To determine whether Trem2 regulated the biological behaviors of osteoclasts in periodontitis, the osteoclast-specific *Trem2* conditional knockout mice (*c*KO mice) were generated. Immunofluorescence staining displayed the reduced number of $CTSK^+$ osteoclasts, and the disappeared co-localization with Trem2 in *c*KO mice with periodontitis (Fig. S1A, B). Alveolar bone remodeling of control mice ($Trem2^{flox/flox}$) in periodontitis exhibited significant resorption of bone in the areas of RF and AS (Fig. 2A, left). Although the bone loss was also observed in *c*KO mice with periodontitis, the extent of bone resorption volume was moderate in *Trem2 c*KO mice as compared to that in control mice, along with the same changes shown in quantitative measurement parameters, including bone mineral density (BMD) and bone volume density (BV/TV) (Fig. 2A, B). The quantification of bone resorption in areas of bone plates and RF exhibited similar results (Fig. 2C). Furthermore, the hematoxylin and eosin (H&E) and tartrate-resistant acid phosphatase (TRAP) staining revealed the remaining alveolar bone and notably reduced osteoclastogenesis in *c*KO mice with periodontitis as compared to that in the control mice (Fig. 2D). The histomorphometric analysis of the bone also demonstrated that compared to control mice, the *c*KO mice displayed significantly lower levels of bone resorption-related parameters (erosion surface/bone surface (ES/BS), osteoclast number/bone surface (Oc.N/BS), and osteoclast surface/bone surface (Oc.S/BS)) in both RF and AS areas with periodontitis (Fig. 2E). Interestingly, although markedly alleviated bone loss occurred in periodontitis in the *c*KO mice as compared to the control mice, distinct changes were not detected in the physiological alveolar bone remodeling in the contralateral side of *c*KO mice (Fig. 2A, B). We also assessed the bone phenotypes between wild-type (WT) and *Trem2*-KO mice with periodontitis and did not find any significant changes in the alveolar bone loss and bone resorption-related parameters between the two groups (Fig. S2A–D).

2.3. Trem2 mediates osteoclastogenesis through in vitro simulation of periodontitis microenvironment by three-dimensional (3D) co-culture system

To simulate periodontitis and normal periodontal microenvironment in vitro, we constructed a 3D culture system composed of mouse gingival epithelial cells, gingival fibroblasts, and periodontal ligament fibroblasts with the applications of *P.g*-lipopolysaccharide (LPS) or an equivalent amount of phosphate-buffered saline (PBS), respectively. As the pattern image is shown in Fig. 3A, the supernatants were collected, LPS was removed, and grouped as inflammatory supernatant (IS) and normal supernatant (N.S.), respectively. The supernatants of IS and NS were treated with RANKL (50 ng/mL) to facilitate the osteoclastogenic differentiation of WT and *Trem2*-KO BMMs. TRAP and phalloidin staining displayed the larger $TRAP^+$ osteoclasts and F-actin ring for IS as compared to that for NS in the WT BMMs. However, significantly fewer and smaller $TRAP^+$ cells along with immature F-actin ring were observed in *Trem2*-KO BMMs, irrespective of whether the IS was introduced (Fig. 3B). The bone resorption assay suggested that the introduction of inflammatory supernatant significantly enhanced the osteolytic ability of osteoclasts; however, this effect was not reflected in *Trem2*-KO BMMs (Fig. 3C). The DHE-based detection of intracellular ROS level was carried out and a significantly increased intracellular ROS level was detected in the WT group introduced by IS (Fig. 3D). However, with the knockout of Trem2, the introduction of IS failed to trigger the increase in intracellular ROS, which remained at a low level. Besides, the inflammatory supernatant enhanced the proliferation of BMMs by BrdU incorporation; however, no significant changes were observed between WT and *Trem2*-KO BMMs (Fig. 3E). In addition, we also detected the transcriptional level of osteoclastogenesis-related genes (*Trap*, *Ctsk*, *Ctr*, *V-ATPase*, and *Dc-stamp*) by RT-qPCR (Fig. 3F), the phosphorylation level of p-Syk, and the levels of TREM2 and osteoclastogenesis-related transcription factors (c-Fos and NFATc1) by Western blotting (WB) (Fig. 3G); similar changes were observed in the mRNA and protein levels. These results indicated that the osteoclastogenic differentiation of BMMs was blocked with the knockout of Trem2 and the pro-osteoclastogenic function of IS displayed in a Trem2-dependent manner.

2.4. Trem2/DAP12-mediated Syk-dependent intracellular ROS amplification cascade activates RANKL-induced NF-κB signaling in osteoclastogenesis

To identify the specific mechanism underlying Trem2 in osteoclastogenesis, adenovirus-mediated Trem2-overexpressed BMMs (Ad*Trem2*, Fig. 4A) and *Trem2*-KO BMMs were utilized. The results of co-immunoprecipitation (Co-IP) suggested that the level of Trem2 protein did not affect the RANKL-induced binding of TRAF6 to RANK (Fig. 4B), but directly affected the formation of the TREM2/DAP12 complex and the recruitment and phosphorylation of Syk (Fig. 4C). Taken together, the RANKL-RANK/TRAF6 axis-induced ROS production was not affected. Furthermore, the level of Trem2 protein was positively correlated with the levels of RANKL-induced phosphorylated P65 and IκBα, and directly affected the nuclear translocation of P65 (Fig. 4D–F). The measurement of Syk kinase activity and luciferase reporter assay suggested that the Syk activity and transcriptional activities of NF-κB and NFATc1 were positively correlated with the level of Trem2 protein (Fig. 4G, H). These findings suggested that Trem2 affected NF-κB signaling and NFATc1 transcription activity in a Syk-dependent manner.

To determine whether the Trem2/DAP12/Syk axis played a role in regulating ROS production during osteoclastogenesis, we detected RANKL-induced intracellular ROS levels of BMMs in WT, *Trem2*-KO, AdCtrl, and Ad*Trem2*, respectively. In *Trem2*-KO BMMs, the intracellular ROS level was low with ROS notably higher in the Ad*Trem2* groups than that in AdCtrl group (Fig. 4I).

To further confirm that intracellular ROS level was regulated via Syk recruited by Trem2/DAP12 complex, the Syk inhibitor (BAY61-3606) was applied, which decreases of kinase activity significantly in both groups, AdCtrl and Ad*Trem2* (Fig. 4J). In addition, with the application of BAY61-3606, the RANKL-induced ROS production was maintained at a low level in a Trem2-independent manner (Fig. 4K). Furthermore, the blocked nuclear translocation of P65 (Fig. 4L) significantly decreased the transcriptional activities of NF-κB (Fig. 4M) and impaired the maturation of osteoclasts (Fig. 4R), suggesting that the Trem2/DAP12-mediated Syk-dependent intracellular ROS amplification cascade was necessary for osteoclastogenesis.

To clarify whether this regulatory mechanism also existed in the periodontitis microenvironment, BAY61-3606 was applied to groups of WT + NS and WT + IS The BMMs also provided similar results as above (Fig. 4N–Q, S), indicating that a similar regulatory mechanism was applicable in the osteoclastogenesis of periodontitis.

2.5. β-amyloid oligomer is a major promoter of osteoclastogenesis in vitro in a Trem2-dependent manner

The enzyme-linked immunosorbent assay (ELISA) was used to detect the levels of β-amyloid 40, 42 ($A\beta_{40}$, $A\beta_{42}$) and oligomers (Aβo) in serum and gingival crevicular fluid (GCF) in mouse periodontitis model on days 7 and 14, with the levels of $A\beta_{42}$ and Aβo positively correlated with the modeling period (Fig. 5A, B). In addition, the upregulation of $A\beta_{42}$ and Aβo could also be detected in the inflammatory supernatant of 3D culture system stimulated by *P.g*-LPS (Fig. 5C). To evaluate whether upregulated β-amyloid plays a major role in promoting osteoclastogenesis in the inflammatory supernatant, $A\beta_{42}$ neutralizing antibody (neutralizing both monomers and oligomers) was applied to pretreat the supernatant. Compared to the IS without pretreatment, the decreased

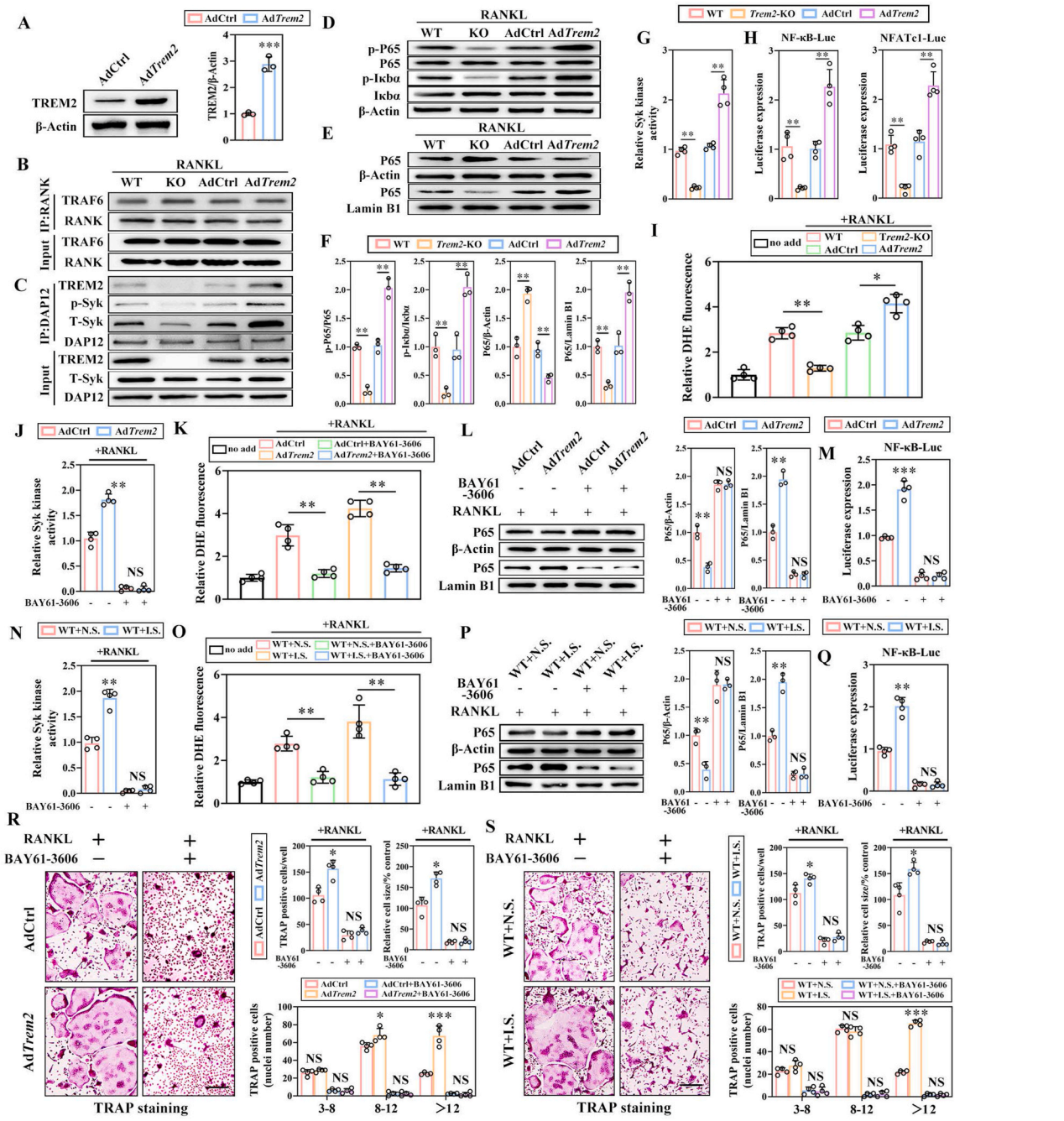

Fig. 4. Trem2/DAP12-mediated Syk-dependent intracellular ROS amplification cascade is necessary for osteoclastogenesis through the upregulation of RANKL-induced NF-κB signaling. **(A)** BMMs were transfected with AdCtrl and Ad*Trem2* for 48 h, and the expression of TREM2 analyzed by WB (left) and quantification (right) ($n = 3$). **(B)** Co-IP was performed to examine the combination state between TRAF6 and RANK, **(C)** along with TREM2, DAP12, and p-Syk in the BMMs stimulated by RANKL for 30 min ($n = 3$). **(D)** The expression and phosphorylation level of IκBα and P65 were measured by WB ($n = 3$). **(E)** The cytoplasmic and nuclear proteins were extracted separately for the detection of nuclear translocation of P65 ($n = 3$). **(F)** The quantification of D (left) and E (right). **(G)** The Syk kinase activity was measured and normalized against WT BMMs with RANKL-induced stimulation of 30 min, set at 1 ($n = 4$). **(H)** The transcription activity of NF-κB and NFATc1 was measured by luciferase reporter assay and normalized against WT BMMs ($n = 4$). **(I)** The fluorescence intensities of DHE in BMMs stimulated with RANKL, normalized to the value of WT group, which was set at 1 ($n = 4$). BMMs of AdCtrl and Ad*Trem2* were pre-treated with BAY61-3606 for 2 h before stimulated by RANKL and the Syk kinase activity **(J)**, the DHE intensity normalized to the value of AdCtrl group **(K)**, the P65 nuclear translocation **(L, left)** and the quantitative analysis **(L, right)**, combined with the transcription activity of NF-κB **(M)** were measured, normalized to the value of AdCtrl group without the pre-treatment of BAY61-3606 ($n = 4$). Similarly, BMMs of WT + NS and WT + IS were pre-treated with BAY61-3606 and the Syk kinase activity **(N)**, the relative DHE intensity **(O)**, the P65 nuclear translocation **(P, left)**, and the quantitative analysis **(P, right)**, combined with the transcription activity of NF-κB **(Q)** were measured ($n = 4$). **(R)** Representative images for TRAP$^+$ osteoclasts in AdCtrl or Ad*Trem2* OCs treated with or without BAY61-3606, respectively (left). Scale bar, 100 μm. The cell number, nuclei number, and relative cell size of the TRAP$^+$ OCs were quantified (right) ($n = 4$). **(S)** Representative images for TRAP$^+$ osteoclasts in BAY61-3606 pre-treated WT + NS or WT + I.S OCs (left), with quantification (right). Scale bar, 100 μm ($n = 4$). Values present mean ± SEM: NS, not significant; *$P < 0.05$, **$P < 0.01$, and ***$P < 0.001$ by one-way ANOVA (F, G, H, I) and unpaired two-tailed Student's t-test.

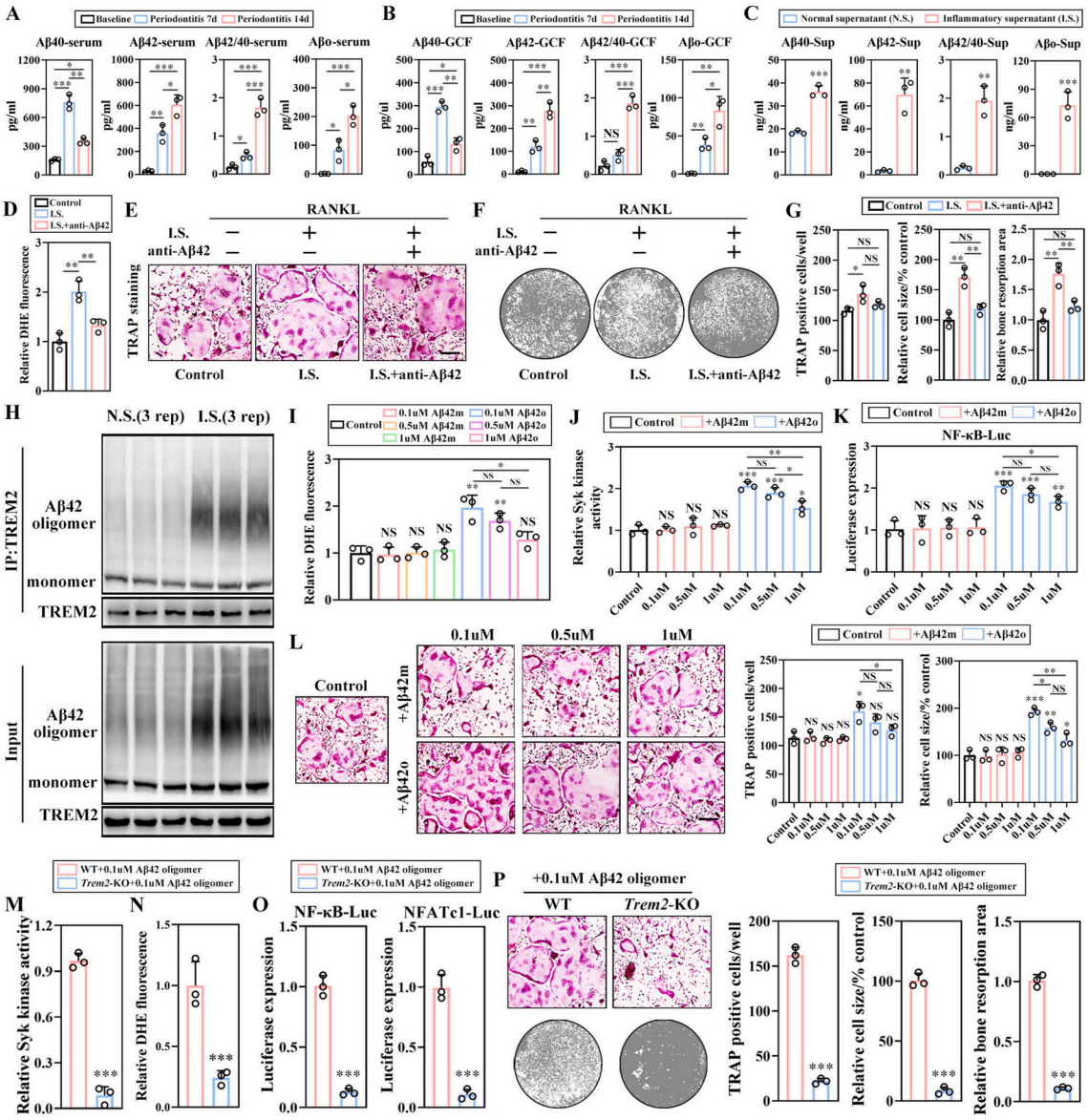

Fig. 5. β-amyloid oligomer is a promoter of osteoclastogenesis in vitro in a Trem2-dependent manner. **(A)** The concentrations of β-amyloid 40 ($A\beta_{40}$), 42 ($A\beta_{42}$), and oligomer (Aβo) in the serum of control and periodontitis mouse models at days 7 and 14 were measured by ELISA ($n = 3$). **(B)** The levels of $A\beta_{40}$, $A\beta_{42}$, and Aβo in gingival crevicular fluid (GCF) ($n = 3$). **(C)** The levels of $A\beta_{40}$, $A\beta_{42}$, and Aβo in NS and IS ($n = 3$). **(D)** The ROS levels in BMMs pre-treated by anti-$A\beta_{42}$ neutralizing antibody for 2h ($n = 3$). **(E)** Representative images for $TRAP^+$ osteoclasts in the f Control, IS, and IS + anti-$A\beta_{42}$ with or without the applications of $A\beta_{42}$ neutralizing antibody groups. Scale bar, 100 μm ($n = 3$). **(F)** Representative images for bone resorption by OCs ($n = 3$). **(G)** The quantification of $TRAP^+$ cell number, size, and bone resorption area of the $TRAP^+$ OCs ($n = 3$). **(H)** The association between TREM2 and β-amyloids in NS and IS by Co-IP ($n = 3$). **(I)** DHE intensities with the stimulations of $A\beta_{42}$m or $A\beta_{42}$o at different concentrations (0.1, 0.5, and 1 mM) combined with RANKL, normalized to the value of Control, which was set at 1 ($n = 4$). **(J)** The Syk activities of BMMs stimulated by Aβ42 m or Aβ42o at different concentrations (0.1, 0.5, 1 mM), in combination with RANKL. The relative expression levels were normalized against the control, which was set at 1 ($n = 3$). **(K)** The transcriptional activities of NF-κB with normalization against the control, which was set at 1 ($n = 3$). **(L)** Representative images for mature OCs induced with the applications of $A\beta_{42}$m or $A\beta_{42}$o at different doses, along with RANKL (left). Scale bar, 100 μm ($n = 3$). The quantitative analysis is shown (right). The Syk kinase activity **(M)**, the DHE intensity **(N)**, along with the transcriptional activities of NF-κB and NFATc1 **(O)** of WT and *Trem2*-KO BMMs with combined stimulations of RANKL and 0.1 mM $A\beta_{42}$o ($n = 3$). The maturation and bone resorption capabilities of OCs, stimulated by the combination of RANKL and 0.1 mM $A\beta_{42}$o **(P, left)** with quantification **(P, right)**. Scale bar, 100 μm ($n = 3$). Values present mean ± SEM: N.S., not significant; $^*P < 0.05$, $^{**}P < 0.01$, and $^{***}P < 0.001$ by one-way ANOVA (D, G, I, J, K, L) and unpaired two-tailed Student's t-test.

ROS level (Fig. 5D), smaller $TRAP^+$ osteoclasts, and impaired osteolytic function (Fig. 5E–G) could be observed. To evaluate the interaction between TREM2 and Aβ in periodontitis microenvironment, Co-IP was applied and it was demonstrated that both $A\beta_{42}$ monomer ($A\beta_{42}$m) and Aβ oligomer could interact with TREM2 directly (Fig. 5H). In order to identify the type of Aβ in major osteoclastogenic promoting capabilities, we measured the ROS levels, the Syk kinase activity, the transcriptional activity of NF-κB, and the osteoclasts maturation by TRAP staining in BMMs stimulated by the combination of RANKL and $A\beta_{42}$ monomer or Aβo at various concentrations (0.1, 0.5, and 1 mM, respectively) (Fig. 5I–L). The results displayed that the stimulation of $A\beta_{42}$m did not exert any significant effect on promoting osteoclastogenesis as compared to the control group, while the Aβo significantly promoted the differentiation of osteoclasts at the optimum concentration of 0.1 mM. To confirm whether Aβo plays a role via interaction with TREM2, 0.1 mM Aβo was applied to WT and *Trem2*-KO BMMs, respectively. It was found that the Syk activity, the ROS level, the transcriptional activity of NF-κB, and NFATc1 in the *Trem2*-KO group were significantly lower as

compared to the WT group, along with the severely affected differentiation and osteolytic function of osteoclasts (Fig. 5M–P). These results suggested that Aβo might exert an in vitro osteoclastogenic promoting function in a Trem2-dependent manner.

2.6. β-amyloid oligomer aggravates bone resorption in an osteoclast-specific Trem2-dependent manner in periodontitis microenvironment

To clarify the in vivo biological effects of the interaction between Aβo and TREM2 on alveolar bone remodeling in periodontitis, Tg2576 mice, overexpressing human β-amyloid precursor protein (hAPP), were mated with *Trem2*$^{flox/flox}$ and *Trem2-c*KO mice, respectively. According to the micro-CT images, compared to the control group (*Trem2*$^{flox/flox}$), the quantification parameters of APP-overexpressing mice (*APP*$^{+/-}$, *Trem2*$^{flox/flox}$), including BMD and BV/TV, were significantly lower and underwent a severe reduction with periodontitis, along with the occurrence of severe bone resorption in areas of RF and buccal and lingual plates (Fig. 6A middle, B, C). However, the combination of overexpressed APP and osteoclast-specific Trem2 knockout (*APP*$^{+/-}$, *Trem2-c*KO) showed alleviated bone resorption as compared to the control group (Fig. 6A right, B, C). H&E staining displayed abundant residual alveolar bones in *APP*$^{+/-}$ and *Trem2-c*KO but fewer in *APP*$^{+/-}$

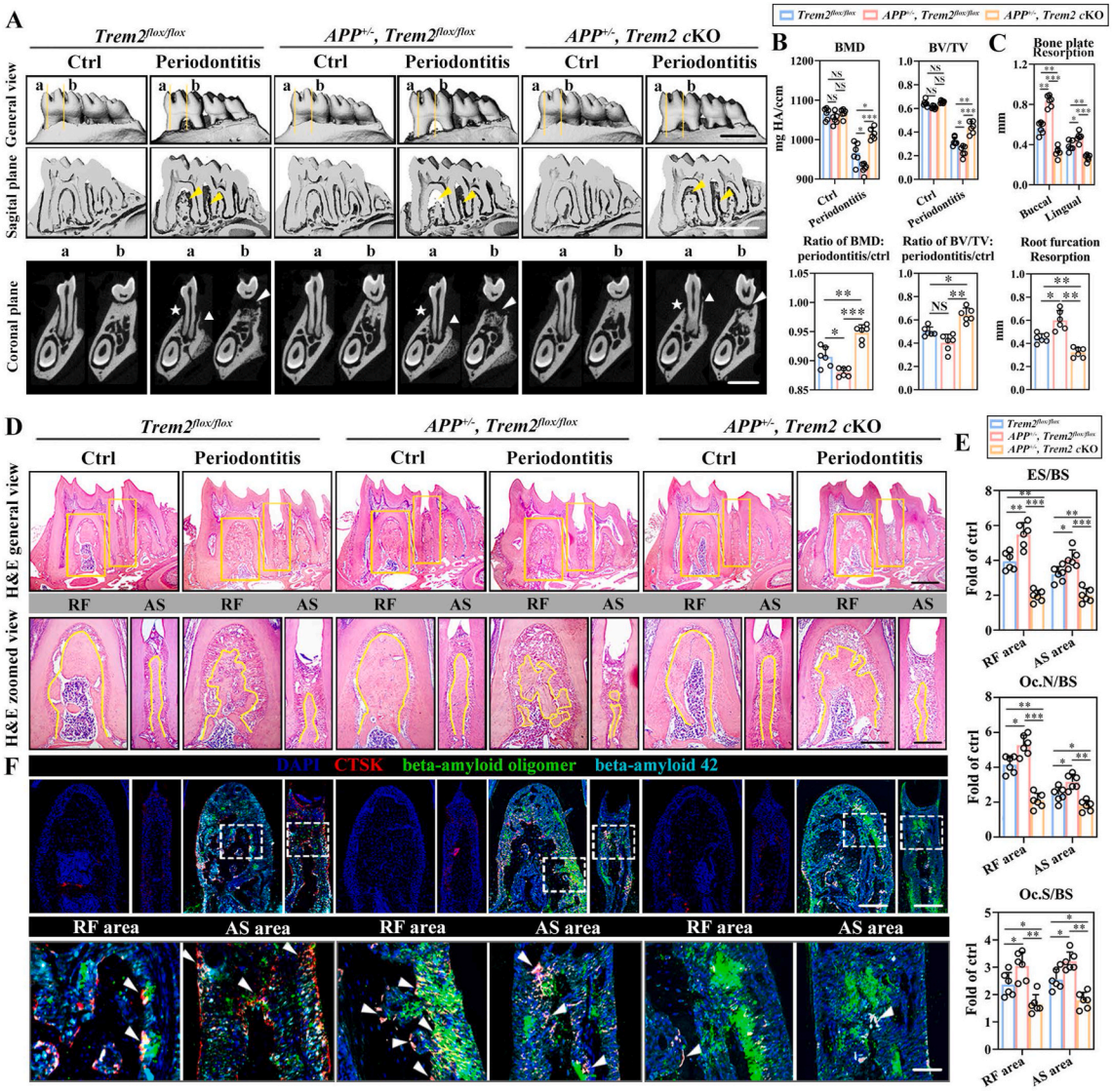

Fig. 6. β-amyloid oligomer aggravates bone resorption in an osteoclast-specific Trem2-dependent manner in the periodontitis microenvironment. **(A)** Representative micro-CT images of mice mandibles subjected to periodontitis with a general view (top), sagittal view (middle), and coronal view (bottom). Resorptions in the areas of RF and AS, observed in the sagittal plane, are indicated by the yellow arrows (middle). The coronal plane was cut in the center of the M1 mesial root and RF, respectively, shown as planes a and b (top), with the white triangles, stars, and arrows (bottom) indicating the buccal, lingual bone plates, and RF area, respectively ($n = 6$). **(B)** Bone histomorphometric analysis of BMD and BV/TV (top) in the alveolar bones from *Trem2*$^{flox/flox}$, *APP*$^{+/-}$, *Trem2*$^{flox/flox}$, and *APP*$^{+/-}$, *Trem2-c*KO mice and calculated ratio of periodontitis to their respective contralateral sides (bottom) ($n = 6$). **(C)** Measurements of bone resorption levels in the bone plates of buccal and lingual sides and in the area of RF ($n = 6$). **(D)** H&E staining of mandibles from periodontitis and control mice, with the general view (top) and enlarged views of RF and AS indicated by the yellow square (top). In addition, the outline of alveolar bones is depicted by the yellow line (bottom) ($n = 6$). Scale bar, 250 μm (top), 100 μm (bottom). **(E)** Bone resorption parameters of alveolar bones subjected to periodontitis, including ES/BS, Oc.N/BS, and Oc.S/BS, with the normalization against their contralateral controls, which were set at 1 ($n = 6$). **(F)** Confocal microscopy of mIF images of RF (left) and AS (right) areas in control and periodontitis mice, using DAPI, anti-CTSK, anti-b-amyloid 42 and anti-b-amyloid oligomer antibodies (top). Scale bar, 100 μm. The enlarged views of RF and AS were exhibited (bottom), which are indicated by the white square (top) and the osteoclasts are indicated by the white arrows. Scale bar, 50 μm ($n = 6$). Values present mean ± SEM: N.S., not significant; $^{*}P < 0.05$, $^{**}P < 0.01$, and $^{***}P < 0.001$ by one-way ANOVA (**B**, **C**) and unpaired two-tailed Student's t-test.

and *Trem2*$^{flox/flox}$ mice as compared to the remaining bone in the control group (Fig. 6D), with respect to the bone resorption-related parameters (ES/BS, Oc.N/BS, Oc.S/BS) (Fig. 6E).

According to multiple immunofluorescence (mIF) assay, the overexpression of hAPP (*APP*$^{+/-}$, *Trem2*$^{flox/flox}$) led to increased expression of $A\beta_{42}$ and Aβo in periodontitis, along with the formation of more CTSK^{+} osteoclasts as compared to the control group. However, fewer and smaller CTSK^{+} osteoclasts, combined with lesser co-localization with Aβo precipitation, were presented in *APP*$^{+/-}$, *Trem2*-cKO mice. Collectively, these data suggested that β-amyloid oligomer, induced in periodontitis microenvironment, enhances alveolar bone resorption in an osteoclast-specific Trem2-dependent manner (Fig. 6F).

2.7. The pattern graph of the pathological changes

The pattern graph depicted the pathological changes at the tissue level (Fig. 7A) and the variations in intracellular signaling of osteoclastogenesis (Fig. 7B) in periodontitis.

3. Discussion

Bone remodeling is a finely regulated process through the balance between osteoblasts-induced bone formation and osteoclasts-induced bone resorption, and their dysregulation is closely associated with several diseases of the skeletal system [18]. In periodontitis, the enhanced alveolar bone loss was brought about by aggravated

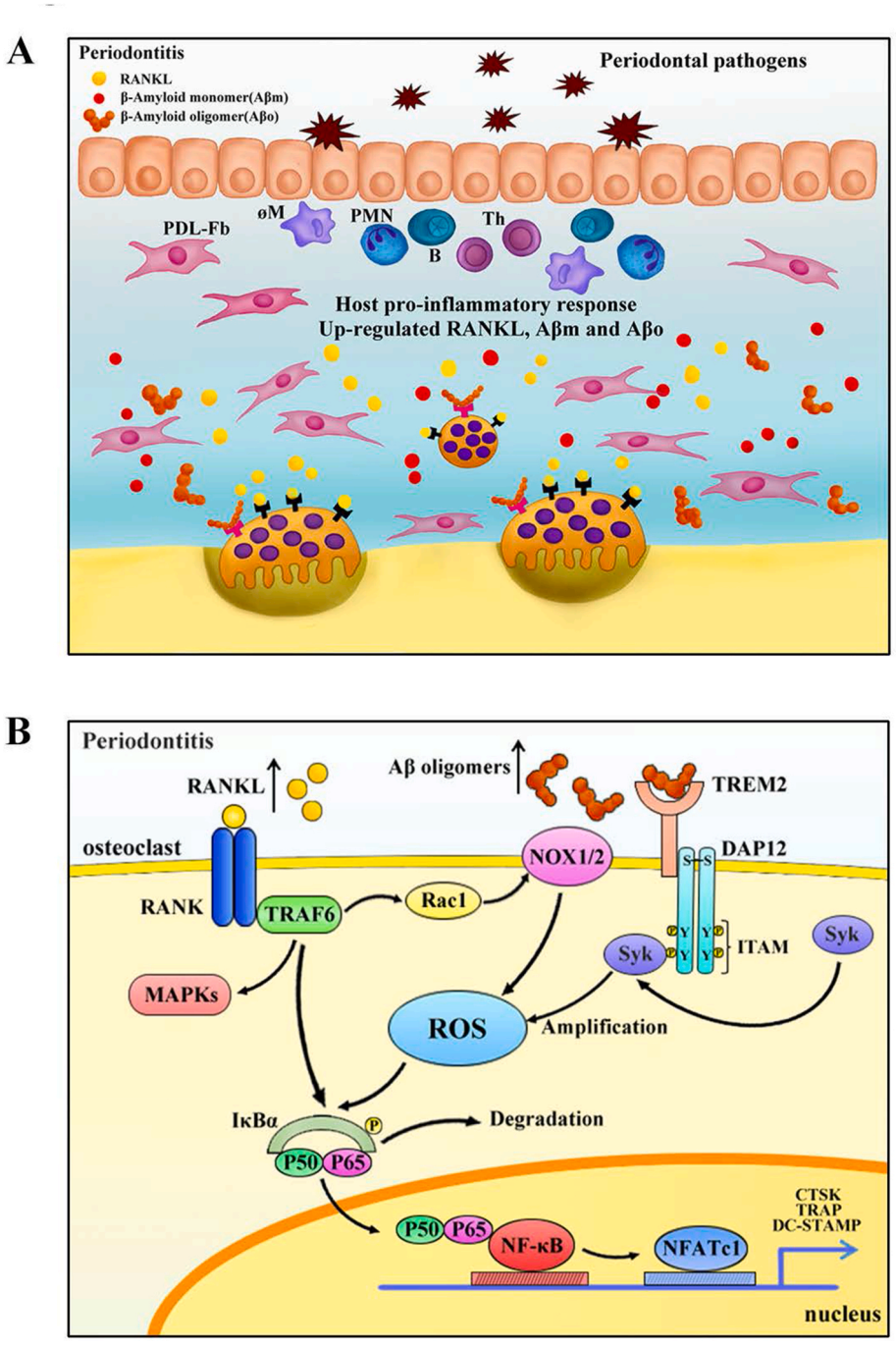

Fig.7. The pattern graph of the pathological changes. (A) The pattern graph of the pathological changes of periodontitis at the tissue level. **(B)** The pattern graph of the signaling variations in the osteoclasts of periodontitis microenvironment.

differentiation and activities of osteoclasts [1]. The regulation of osteoclast differentiation is a multi-step process. Divergent from the physiological state, the complex regulatory network of bone resorption was formed by the cross-interaction of various ligands, receptors, signal molecules, and transcription factors in periodontitis microenvironment [8]. Therefore, identifying critical mediators of osteoclast differentiation in periodontitis and clarifying their biological functions could provide novel treatment strategies. In this study, we first performed RNA-seq on alveolar bone samples from healthy donors and patients diagnosed with chronic periodontitis. The results of GSEA showed that the expression pattern of alveolar bone remodeling under periodontitis was primarily characterized by enhanced oxidation, inflammation, and osteoclast differentiation-related signals and biological processes. Combined with the results of differential expression analysis and GSEA, we identified TREM2 ($log_2FC = 4.66$, padj $= 1.8 \times 10^{-5}$) as the putative key regulator associated with the biological patterns mentioned above. In addition, we found the notably upregulated level of TREM2 protein in both human alveolar bone and mouse periodontal tissues with periodontitis, suggesting that Trem2 might be closely related to the alveolar bone remodeling in periodontitis.

Trem2 is a receptor molecule that mediates immune responses and is widely distributed on the surface of myeloid cells. It is known to function in mediating phagocytosis and inflammatory response [19,20], regulating tissue and organ fibrosis [21] and lipid metabolism [22]. With the knowledge of pathogenesis and phenotype of Nasu-Hakola disease, a genetic disease caused by mutations in Trem2 or DAP12, the functional correlation was established between Trem2 and osteoclastogenesis, which proved Trem2 to be a vital co-receptor for osteoclast differentiation [9]. Interestingly, the phenotype of the disease mainly involved organs developed with the mechanism of endochondral ossification but not craniomaxillofacial bones based on intramembranous ossification [10], which was similar to our findings in the mice models. Physiologically, compared to the WT mice, the *Trem2*-KO and *Trem2*-*c*KO mice were characterized by thickened cortical bone and higher trabecular bone mass (Fig. S3A, B) in femurs, but no significant changes occurred in the alveolar bones of mandibles. However, pathologically, *Trem2*-*c*KO mice exhibited significantly more residual alveolar bones, while no significant discrepancies were observed in the bone resorption between *Trem2*-KO and WT mice. Based on the differences in the phenotypes and cell types with *Trem2*-KO in vivo between *Trem2*-KO and *Trem2*-*c*KO mice, we speculated other types of Trem2-positive cells that played regulatory roles in the pathological alveolar bone remodeling in periodontitis microenvironment. To simulate the periodontitis microenvironment for osteoclastogenesis in vitro, we constructed a 3D culture system composed of gingival epithelial cells, gingival fibroblasts, and periodontal ligament fibroblasts. Th *P.g*-LPS or equivalent amount of PBS was input in the system to acquire the inflammatory and normal supernatants, respectively, with the former significantly enhancing the osteoclastogenesis of WT BMMs. However, the differentiation of *Trem2*-KO BMMs was not observed despite the application of inflammatory supernatant. These data indicated that Trem2 is essential in mediating the differentiation and maturation of osteoclasts in periodontitis.

ROS is a single-electron reduction product of oxygen. The appropriate concentration of intracellular ROS regulated the biological functions of the cell [23]. According to the current understanding, the RANKL-RANK-TRAF6-Rac1-Nox signal axis was considered to be the main ROS production cascade in osteoclastogenesis [13]. However, due to the requirements of costimulation signals provided by ITAM sequence in osteoclast differentiation, it was suggested that other regulatory signals might exist in ROS production during this process. As a major provider for costimulation signals, Trem2/DAP12 complex is capable of recruiting and phosphorylating Syk. In neutrophils and macrophages, Syk is recruited and activated by ITAM in FcRγ; subsequently, it induces the ROS burst [24]. Our results showed that compared to the WT group, the RANKL-induced intracellular ROS level of *Trem2*-KO BMMs was maintained at a low level, and the expression level of Trem2 was positively correlated with the recruitment and phosphorylation of Syk; however, it not affect the interaction between RANK and TRAF6. Moreover, the application of Syk blocker BAY61-3606 further proved that the ascending ROS level was mediated through the activated Syk recruited by Trem2/DAP12. Interestingly, the Trem2/DAP12-mediated osteoclastogenic ROS production also shared the characteristics of ROS outbreaks with other immune cells of hematopoietic sources [25]. These findings proved that the Trem2/DAP12-mediated Syk-dependent pathway was another essential osteoclastogenesis-related ROS regulating signal cascade with the characteristics of ROS outbreaks, which might be closely related to the enhanced osteoclast activity in periodontitis.

Based on the correlation between the progression of periodontitis and Alzheimer's disease (AD), we further studied the expression patterns and possible biological functions of Aβ in periodontitis. These results showed that $A\beta_{42}$ and the oligomers of Aβ were significantly upregulated in periodontitis mouse model and widely deposited in the periodontal tissue. In addition, we also detected a high level of Aβ in the inflammatory supernatant stimulated by *P.g*-LPS in the 3D culture system, with the osteoclastogenesis promoting effect alleviated by the neutralizing antibody. We also found that the Aβ oligomer (Aβo) is the main role player in promoting osteoclastogenesis. In the periodontitis microenvironment, Aβ promoted osteoclast differentiation via binding with Trem2 and activating the Trem2-mediated Syk-dependent ROS signal amplification cascade. Furthermore, to clarify the correlation between Aβ and Trem2 under physiological and pathological conditions, Tg2576 mice were mated with *Trem2*-KO and *Trem2*-cKO mice, respectively. Under physiological conditions, the levels of APP and Trem2 did not have any significant effects on alveolar bone remodeling with traces of $A\beta_{42}$ and Aβo detected in the periodontal areas. Pathologically, the APP overexpression leads to increased expression of $A\beta_{42}$ and Aβo, combined with strengthened osteoclastogenesis and alveolar bone loss, while the combination of APP overexpression and osteoclast-specific Trem2 KO exhibited slight bone resorption and less spatial overlap between $CTSK^+$ osteoclasts and Aβo, indicating a significant role of Aβo in promoting bone resorption in an osteoclast-specific Trem2-dependent manner. Interestingly, the $APP^{+/-}$, *Trem2*-KO group was simulated with the pathological base of clinical AD caused by Trem2 dysfunction at the protein level. A similar bone destruction degree in this mouse model was observed in the APP overexpression group, which provided the experimental evidence for the high incidence and susceptibility of periodontitis in patients with Alzheimer's disease (Fig. S4A–D).

Although our findings proved that Trem2 was essential for osteoclastogenesis in periodontitis, several concerns need yet to be addressed: 1) The reason why Trem2 is only functional in the pathological alveolar bone remodeling with periodontitis; 2) Based on the spatial expression pattern of Trem2 in periodontitis, other $Trem2^+$ cell types and their biological behaviors remained to be elucidated in this pathological condition; 3) Since Trem2 could also signal through PI3K-ERK-Ca^{2+} cascade [26], a cross-talk between Ca^{2+} and ROS signaling mediated by Trem2 was speculated in the regulation of osteoclastogenesis; 4) The roles of Aβ in the interactions with other $Trem2^+$ cell types and the putative biological functions. Collectively, Trem2 is a vital regulator for pathological bone remodeling in periodontitis. The $Trem2^+$ osteoclasts were capable of recognizing the Aβo deposited in the pathological microenvironment and signaling via the new cascade, Trem2/DAP12-mediated Syk-dependent pathway; together, these would amplify the intracellular ROS level and regulate osteoclast differentiation. Therefore, the targeted regulation of Trem2 expression in osteoclasts is expected to become a novel target with remarkable potential for the prevention and treatment of bone resorption in periodontitis.

4. Methods

4.1. Mice

Trem2$^{-/-}$ (*Trem2* KO) mice were purchased from Jackson Laboratory, USA (C57BL/6J-Trem2$^{em2Adiuj/J}$). *Trem2*$^{flox/flox}$ mice (C57BL/6J-*Trem2*$^{em2(flox)Smoc}$, Shanghai Model Organisms Center Inc., China) were mated with *Ctsk-Cre* knock-in mice (C57BL/6J-*Ctsk*$^{em1(2A-Cre-Wpre-pA)Smoc}$, Shanghai Model Organisms Center) in which the *Cre* recombinase gene was specifically expressed in osteoclasts. *Ctsk-Cre*$^{+/-}$, *Trem2*$^{flox/flox}$ (*Trem2* cKO) and *Ctsk-Cre*$^{-/-}$, *Trem2*$^{flox/flox}$ (normal littermates) mice were generated by mating *Ctsk-Cre*$^{-/-}$, *Trem2*$^{flox/flox}$ male mice with *Ctsk-Cre*$^{+/-}$, *Trem2*$^{flox/+}$ female mice. Heterozygous Tg2576 mice (*APP*$^{+/-}$) overexpressing the human Swedish APP mutation (B6; SJL-Tg (APPSWE)2576Kha, Taconic Biosciences, Germany) on a mixed C57BL/6×SJL background were crossed with *Ctsk-Cre*$^{+/-}$, *Trem2*$^{flox/flox}$ mice to generate three groups of mice: *APP*$^{-/-}$, *Ctsk-Cre*$^{-/-}$, *Trem2*$^{flox/flox}$ (normal littermates); *APP*$^{+/-}$, *Ctsk-Cre*$^{-/-}$, *Trem2*$^{flox/flox}$ (Tg2576); *APP*$^{+/-}$, *Ctsk-Cre*$^{+/-}$, *Trem2*$^{flox/flox}$ (Tg2576×*Trem2* cKO). In the current study, 2-month-old male mice were used for animal experiments with at least three biological repeats in each group. The mice were maintained in accordance with the National Institutes of Health's *Guide for the Care and Use of Laboratory Animals*, and the study protocols were approved by The Animal Care and Use Committee of Tongji University.

4.2. Reagents and antibodies

Antibodies used in this study are listed in Supplementary Table 1. The *P. gingivalis* LPS (*P.g*-LPS) was purchased from Sigma. The selective Syk inhibitor BAY61-3606 was purchased from GLPBIO. The $A\beta_{1-42}$ was purchased from AnaSpec. The $A\beta_{42}$ monomer and $A\beta_{42}$ oligomer were prepared, as described previously [27]. Briefly, the peptides of $A\beta_{1-42}$ were dissolved in DMSO (5 mM) and diluted to 100 μM with cold phenol-free α-MEM basic medium and sonicated for 10 min to make $A\beta_{42}$ monomer. To obtain $A\beta_{42}$ oligomers, the sonicated peptides were incubated at 22 °C for 16 h, followed by 24 h incubation at 4 °C and centrifugation at 16000×*g* for 15 min to collect the supernatant, which was considered to be $A\beta_{42}$ oligomer.

4.3. Human alveolar bone specimens

Specimens of alveolar bones were obtained from 5 healthy donors (30–40-years-old, male, no history of alcohol, smoking, and systemic diseases) whose alveolar bones of upper premolars needed to be trimmed for the following restoration by coronal lengthening surgery. In the case of specimens with chronic periodontitis, 5 donors were diagnosed with upper front teeth chronic periodontitis (30–40-years-old, male, no history of alcohol, smoking, and systemic diseases with average attachment loss of 4–5 mm) who needed to undergo tooth extraction and alveolar ridge preparation for the upcoming implant surgery. The specimens were collected at the Department of Oral and Maxillofacial Surgery of the Affiliated Stomatology hospital of Tongji University (Shanghai, China). None of the donors received any preoperative treatment, and all the donors signed informed consent forms. This study was approved by the Ethics Committee of the Affiliated Stomatological Hospital of Tongji University, Shanghai, China and conducted in accordance with the Declaration of Helsinki, 1975 revised in 2013.

4.4. Mouse experimental periodontitis models

In mice modeling, a 6-0 ligature was passed through the space between the mandibular first and second molars and then tightened around the subgingival region of the first molar crown. The ligature was retained for 2 weeks.

4.5. Preparation of mouse BMMs and osteoclast differentiation

The whole bone marrow cells were collected from the long bones of 2-month-old C57BL/6 (WT) or *Trem2*$^{-/-}$ (*Trem2*-KO) mice (including femurs and tibias) and cultured in α-MEM complete medium containing 10% FBS and 100 U/mL penicillin-streptomycin for 24 h. Then, the non-adherent cells in the supernatant were isolated and cultured in α-MEM complete medium with 30 ng/mL M-CSF for 3 days, with the adherent cells used as bone marrow-derived macrophages (BMMs). To generate osteoclasts, BMMs were digested, calculated, and seeded into 96 or 24-well plates at a density of 1×10^4 or 5×10^4/well in the presence of complete α-MEM medium containing 30 ng/mL M-CSF and 50 ng/mL RANKL. The media was changed every 2 days and cultured for 4 days until mature osteoclasts were formed. According to the previous studies [28], cells were fixed with 4% paraformaldehyde, permeabilized with 0.1% Triton X-100 and stained by rhodamine-phalloidin to identify the actin ring formation of osteoclasts. In addition, the TRAP activity of osteoclasts was measured by TRAP staining and TRAP$^+$ cells with more than three nuclei counted as osteoclasts.

4.6. 3D co-culture system and periodontitis microenvironment-simulated osteoclastogenic differentiation

The primary mouse gingival epithelial cells, gingival fibroblasts, and periodontal ligament fibroblasts were obtained, as described previously [29–31]. The cultivation of the cells and construction of the 3D co-culture model have been elaborated previously, with modifications in our study [32]. The model was stimulated with *P.g*-LPS (10 μg/mL) for 48 h at 37 °C in a 5% CO_2 atmosphere with the application of equivalent amounts of PBS as control. Then, the supernatants were collected and subjected to centrifugation at 3000×*g*, 10 min at 4 °C. The endotoxin removing columns (Detoxi-Gel^{TM}, ThermoFisher) were used to eliminate the LPS in the supernatants. On the day of osteoclastogenic induction of BMMs, the LPS-free supernatants of the inflammatory (IS) or control groups (NS) were used as the culture media supplemented with RANKL (50 ng/mL) and changed every 2 days.

4.7. In vitro proliferation assay

Proliferation was assessed in BMMs from C57BL/6 (WT) and *Trem2*$^{-/-}$ (*Trem2*-KO) grown in M-CSF (30 ng/mL) for 3 days, using the cell proliferation BrdU kit (Roche). The absorbance was measured at 450 nm in accordance with the manufacturer's instructions.

4.8. Bone resorption assay

24-well bone resorption plates coated with hydroxyapatite were used for the detection of the osteolytic function of osteoclasts. BMMs of C57BL/6 (WT) and *Trem2*$^{-/-}$ (Trem2 KO) mice or transfected by AdCtrl or Ad*Trem2,* were obtained, as described previously. The cells were seeded in the plates at the density of 5×10^4/well with the presence of complete α-MEM medium containing 30 ng/mL M-CSF and 50 ng/mL RANKL. In simulating the periodontitis microenvironment in vitro, the NS or IS, combined with 50 ng/mL RANKL, were used as the culture medium, as described previously. For all groups in the study, the cells were cultured for 10 days, and the media replaced every 2 days. Then, the cells were brushed off the plates, and the resorption areas were observed in the stereomicroscope (Zeiss) and quantified using Image J software.

4.9. RNA-sequencing

Total RNA was isolated from the alveolar bones of donors using TRIzol reagent (Invitrogen) according to the manufacturers' instructions. The RNA purity was assessed using a NanoVue (GE, USA) and the A260:A280 ratio of each sample was maintained at >1.90. Agilent 2200 Tape Station (Agilent Technologies) was used for the evaluation of

RNA integrity with the RNA integrity number (RIN) > 7.0. The library preparation was carried out according to the instructions provided with the Trio RNA-Seq Library Preparation Kit (Nugen Technologies, USA). Subsequently, the purified products were evaluated using the Agilent 2200 TapeStation and Qubit®2.0 (Life Technologies, USA), followed by sequencing (2×150 bp) using a NovaSeq 6000. After removing the raw reads of low-quality, hisat2 was used to align the remaining clean reads to the human genome database (hg38) [33]. The top 50 differentially expressed genes with the lowest padj values were used for the heat map analysis. All genes with TPM >0 were used for the depiction of Volcano plot, Venn plot, and the calculation of PCA. The enrichment of functional gene pathways and biological process of gene oncology were assessed by GSEA using the databases of KEGG pathway (c2.cp.kegg.v6.0.symbols.gmt) and GO-BP (c5.bp.v6.0.symbols.gmt) [34,35].

4.10. RNA extraction and quantitative real-time PCR (qRT-PCR)

The RNA extraction and qRT-PCR are performed, as described previously [36]. The cDNA was amplified by qRT-PCR using the FastStart Essential DNA Green Master Kit (Roche) with a Light Cycler 96 Instrument system (Roche). All the reactions were run in triplicate, and *β-actin* was used as the internal control. The primer sequences were as follows: mouse *β-actin*, 5′-GGCTGTATTCCCCTCCATCG-3′ and 5′-CCAGTTGGTAACAATGCCATGT-3'; mouse *TRAP*, 5′-TGAGGACGTATTCTCTGACCG-3′ and 5′-CACATTGGTCTGTGGGATCTTG-3'; mouse *CTSK*, 5′-CTCGGCGTTTAATTTGGGAGA-3′ and 5′-TCGAGAGGGAGGTATTCTGAGT-3'; mouse *CTR*, 5′-GAGGTTCCTTCTCGTGAACAG-3′ and 5′-AGTCAGTGAGATTGGTAGGAGC-3'; mouse *V-ATPase*, 5′-CTGGTTCGAGGATGCAAAGC-3′, 5′-GTTGCCATAGTCCGTGGTCTG-3'; mouse *DC-STAMP*, 5′-CTGTGTCCTCCCGCTGAATAA-3′, 5′-AGCCGATACAGCAGATAGTCC-3'.

4.11. ELISA

In this study, ELISA was carried out to measure the concentrations of $A\beta_{40}$ peptide, $A\beta_{42}$ peptide, and Aβ oligomer in the GCF and serum specimens from mice at different modeling time points, as well as NS or IS, using the preparation methods described above. The experiments were carried out according to the manufacturers' instructions, and the kits used in the study are listed in Supplementary Table 1.

4.12. Immunoprecipitation (IP) and WB

In this study, IP and WB were carried out according to the previous study [28]. Briefly, for immunoprecipitation, the BMMs of each group were starved in serum-free α-MEM medium for 5 h before stimulated by RANKL (50 ng/mL) for 30 min. Cells were washed twice with ice-cold PBS and lysed with ice-cold IP lysis buffer coupled with 1 mM PMSF and protease inhibitor cocktail with working concentration. The cell lysates were incubated on ice for 30 min before centrifugation at 13000×*g* for 10 min at 4 °C. An equivalent of 50 μL protein A/G-agarose was used to preclear the supernatant and minimize the nonspecific binding for 2 h by gentle rocking. Precleared supernatants of each group containing the same amount of protein was used for immunoprecipitation with specific antibodies by overnight incubation, followed by protein A/G-agarose. The agarose beads were washed five times with the washing buffer and solubilized in 1X loading buffer. For immunoblotting, specific antibodies listed above. For WB, RIPA lysis buffer, coupling with 1 mM PMSF, and protease and phosphatase inhibitors were used for protein extraction, and the nuclear & cytoplasmic extraction kit (Thermo) was used for the separation of nuclear and cytoplasmic proteins. The protocol was followed as described previously [37], and antibodies used in this experiment are listed in Supplementary Table 1.

4.13. Histomorphology analysis and osteoclast activity in vivo

For the morphology observation or detection of protein expression in the periodontal areas of mice mandibles, the mice were perfused with 4% paraformaldehyde and dissected for mandibles that were fixed at 4 °C for 24 h and decalcified with 10% EDTA (pH7.4) for 4 weeks. Then, the samples were embedded in paraffin and sectioned into 4-μm-thick slices. For histomorphological analysis, hematoxylin & eosin (H&E) staining was carried out. TRAP staining was used to examine the bone resorption activities and the activities of osteoclasts in the bone remodeling area. The abbreviations for histomorphometric parameters were as follows: ES, eroded surface; BS, bone surface; Oc.N, osteoclast number; Oc.S, osteoclast surface [38].

4.14. mIF staining

The tyramide signal amplification (TSA) technology was employed in the mIF staining. Briefly, the slices were incubated with the first primary antibody at 37 °C for 1 h, followed by HRP-conjugated secondary antibody at room temperature for 1 h. The tyramide reagent was then used to generate fluorescent precipitate through HRP-substrate reactions. Subsequently, the first-round antibody was stripped and the second-round of another primary antibody started, as described above. DAPI was used to counterstain the nuclei. Antibodies and reagents used in mIF staining are listed in Supplementary Table 1.

4.15. Plasmid and adenovirus

The full-length Trem2 cDNA was amplified by PCR, and cloned into *BamHI* and *MluI* sites of the pADM-FH-GFP expression vector for adenovirus. The adenoviruses carrying the empty vector and the vector integrated with the target gene were packaged using the Adenovirus Generation Kit (Takara), according to the manufacturer's instructions. In our study, the empty adenovirus (AdCtrl) and Trem2 adenovirus (Ad*Trem2*) were used for control and Trem2 overexpression experiments, respectively.

4.16. Measurement of intracellular ROS level

The Dihydroethidium(DHE) cellular ROS detection assay kit (BB-47051-1, Bestbio, China) was used to measure the ROS level in BMMs. Starved BMMs were incubated with dihydroethidium probe (1:100) for 10 min at 37 °C washed before stimulation with RANKL (50 ng/mL) only or combined with stimulations mentioned in the experiments. The fluorescence intensity was measured using 100 μL cell lysates (0.5% Triton X-100) at stimulation time point of 30 min on a hybrid multimode microplate reader (Synergy H1, BioTek) using the excitation/emission wavelengths of 535/610 nm [28].

4.17. Luciferase reporter assay

BMMs were co-transfected transiently with NF-κB-responsive reporter plasmid (pGL-NF-κB-Luc) or NFATc1-responsive plasmid (pGL-NFATc1-Luc) with Renilla luciferase expression plasmid (phRL-TK) using Lipofectamine 3000. After 24 h post-transfection, the cells were harvested following different experiments and stimulation for the measurement of luciferase activity using the Dual-Glo Luciferase Assay System (Promega, Madison, WI, USA). Specific NF-κB or NFATc1 luciferase activity was normalized to that of the internal control.

4.18. In vitro protein kinase assay

ELISA-based Universal Tyrosine Kinase Assay Kit (Genway) was used to detect the tyrosine kinase activity of Syk immunoprecipitates from whole-cell lysates (1 mg of total protein), according to the manufacturer's instructions.

4.19. Analysis of bone morphology

Two-dimensional (2D) images of mandible scanning sections, reconstructed 3D microstructural images, and calculated structural indices were obtained using Micro-CT 50 (Scanco Medical, Switzerland) and affiliated analyzing software at the scanning resolution of 10 μm. Abbreviations used for morphometric parameters were as follows: BMD, bone mineral density; BV/TV, bone volume *vs*. total volume; Bone plate resorption, the resorption height of buccal or lingual plate compared to the contralateral side; RF resorption, the resorption height of alveolar bone in RF area as compared to the contralateral side.

4.20. Statistical analysis

The data were presented in the form of means ± standard error of mean (SEM) from three or more independent experiments mentioned in the legends. For statistical analysis, Student's t-test or Mann-Whitney test was used between the two groups and one-way analysis of variance (ANOVA) was carried out for the comparison between multiple groups with Tukey's post hoc test to assess the differences between specific groups. SPSS 17.0 (IBM) was used to perform all statistical calculations with *P*-values <0.05 considered to be statistically significant (*$P < 0.05$, **$P < 0.01$, ***$P < 0.001$).

Author contributions

Y.W. and Z.W. contributed to the conception of this study, the design of most experiments, and discussion of data. Y.W., L.L., Y.F., S.X. and Z. W. drafted the manuscript. H.W. collected the human samples and accomplished the ethical study. Y.W. performed the RNA-seq and bioinformatics analysis. Y.W. and H.W. carried out the in vivo and in vitro experiments. Y.F., S.X. and H.W. prepared the Aβ monomers and oligomers and performed the in vitro experiments in Fig. 5. Z.W. directed and supervised the project.

Data and materials availability

All relevant data are available from the corresponding authors upon reasonable request.

Declaration of competing interest

We declare that we do not have any commercial or associative interest that represents a conflict of interest in connection with the work submitted.

Acknowledgments

Funding: This work was funded by the National Key Research and Development Program Project of China (No. 2018YFE0202200).

Appendix A. Supplementary data

Supplementary data to this article can be found online at https://doi.org/10.1016/j.redox.2020.101849.

References

[1] S.A. Hienz, S. Paliwal, S. Ivanovski, Mechanisms of bone resorption in periodontitis, J. Immunol. Res. (2015) 615486.
[2] S.S. Dominy, C. Lynch, F. Ermini, M. Benedyk, A. Marczyk, A. Konradi, et al., Porphyromonas gingivalis in Alzheimer's disease brains: evidence for disease causation and treatment with small-molecule inhibitors, Sci. Adv. 5 (1) (2019), eaau3333.
[3] S.E. Choi, C. Sima, A. Pandya, Impact of treating oral disease on preventing vascular diseases: a model-based cost-effectiveness analysis of periodontal treatment among patients with type 2 diabetes, Diabetes Care 43 (3) (2020) 563–571.
[4] M. Xie, Q. Tang, J. Nie, C. Zhang, X. Zhou, S. Yu, et al., BMAL1-Downregulation aggravates Porphyromonas gingivalis-induced atherosclerosis by encouraging oxidative stress, Circ. Res. 126 (6) (2020) e15–e29.
[5] B. Holtfreter, S. Richter, T. Kocher, M. Dörr, H. Völzke, T. Ittermann, et al., Periodontitis is related to lung volumes and airflow limitation: a cross-sectional study, Eur. Respir. J. 42 (6) (2013) 1524–1535.
[6] P.K. Friedman, I.B. Lamster, Tooth loss as a predictor of shortened longevity: exploring the hypothesis, Periodontol. 2000 72 (1) (2016) 142–152.
[7] H. Kato, Y. Takahashi, C. Iseki, R. Igari, H. Sato, H. Sato, et al., Tooth loss-associated cognitive impairment in the elderly: a community-based study in Japan, Int. Med. (Tokyo, Japan) 58 (10) (2019) 1411–1416.
[8] K.H. Park-Min, Mechanisms involved in normal and pathological osteoclastogenesis, Cell. Mol. Life Sci. 75 (14) (2018) 2519–2528.
[9] T. Koga, M. Inui, K. Inoue, S. Kim, A. Suematsu, E. Kobayashi, et al., Costimulatory signals mediated by the ITAM motif cooperate with RANKL for bone homeostasis, Nature 428 (6984) (2004) 758–763.
[10] M.B. Humphrey, M.R. Daws, S.C. Spusta, E.C. Niemi, J.A. Torchia, L.L. Lanier, et al., TREM2, a DAP12-associated receptor, regulates osteoclast differentiation and function, J. Bone Miner. Res. : Offi. J. Am. Soc. Bone Mineral Res. 21 (2) (2006) 237–245.
[11] J.V. Haure-Mirande, M. Audrain, T. Fanutza, S.H. Kim, W.L. Klein, C. Glabe, et al., Deficiency of TYROBP, an adapter protein for TREM2 and CR3 receptors, is neuroprotective in a mouse model of early Alzheimer's pathology, Acta Neuropathol. 134 (5) (2017) 769–788.
[12] J. Paloneva, J. Mandelin, A. Kiialainen, T. Bohling, J. Prudlo, P. Hakola, et al., DAP12/TREM2 deficiency results in impaired osteoclast differentiation and osteoporotic features, J. Exp. Med. 198 (4) (2003) 669–675.
[13] T.S. Agidigbi, C. Kim, Reactive oxygen species in osteoclast differentiation and possible pharmaceutical targets of ROS-mediated osteoclast diseases, Int. J. Mol. Sci. 20 (14) (2019) 3576.
[14] M. Zhu, D. Li, Y. Wu, X. Huang, M. Wu, TREM-2 promotes macrophage-mediated eradication of Pseudomonas aeruginosa via a PI3K/Akt pathway, Scand. J. Immunol. 79 (3) (2014) 187–196.
[15] J. García-Revilla, I.M. Alonso-Bellido, M.A. Burguillos, A.J. Herrera, A. M. Espinosa-Oliva, R. Ruiz, et al., Reformulating pro-oxidant microglia in neurodegeneration, J. Clin. Med. 8 (10) (2019) 1719.
[16] J. Zhao, R. Nussinov, B. Ma, Mechanisms of recognition of amyloid-β (Aβ) monomer, oligomer, and fibril by homologous antibodies, J. Biol. Chem. 292 (44) (2017) 18325–18343.
[17] T.K. Ulland, M. Colonna, TREM2 - a key player in microglial biology and Alzheimer disease, Nat. Rev. Neurol. 14 (11) (2018) 667–675.
[18] R. Baron, M. Kneissel, WNT signaling in bone homeostasis and disease: from human mutations to treatments, Nat. Med. 19 (2) (2013) 179–192.
[19] C. Claes, J. Van Den Daele, R. Boon, S. Schouteden, A. Colombo, L.S. Monasor, et al., Human stem cell-derived monocytes and microglia-like cells reveal impaired amyloid plaque clearance upon heterozygous or homozygous loss of TREM2. Alzheimer's & dementia, J. Alzheimer's Assoc. 15 (3) (2019) 453–464.
[20] C. Claes, J. Van Den Daele, R. Boon, S. Schouteden, A. Colombo, L.S. Monasor, et al., Human induced pluripotent stem cell-derived microglia-like cells harboring TREM2 missense mutations show specific deficits in phagocytosis, Cell Rep. 24 (9) (2018) 2300–2311.
[21] P. Ramachandran, R. Dobie, J.R. Wilson-Kanamori, E.F. Dora, B.E.P. Henderson, N. T. Luu, et al., Resolving the fibrotic niche of human liver cirrhosis at single-cell level, Nature 575 (7783) (2019) 512–518.
[22] D.A. Jaitin, L. Adlung, C.A. Thaiss, A. Weiner, B. Li, H. Descamps, et al., Lipid-associated macrophages control metabolic homeostasis in a trem2-dependent manner, Cell 178 (3) (2019) 686–698, e14.
[23] A. Costa, A. Scholer-Dahirel, F. Mechta-Grigoriou, The role of reactive oxygen species and metabolism on cancer cells and their microenvironment, Semin. Canc. Biol. 25 (2014) 23–32.
[24] G.T. Nguyen, L. Shaban, M. Mack, K.D. Swanson, S.C. Bunnell, D.B. Sykes, et al., SKAP2 is required for defense against K. pneumoniae infection and neutrophil respiratory burst, ELife 9 (2020), e56656.
[25] J.F. Charles, M.B. Humphrey, X. Zhao, E. Quarles, M.C. Nakamura, A. Aderem, et al., The innate immune response to Salmonella enterica serovar Typhimurium by macrophages is dependent on TREM2-DAP12, Infect. Immun. 76 (6) (2008) 2439–2447.
[26] Q. Peng, S. Malhotra, J.A. Torchia, W.G. Kerr, K.M. Coggeshall, M.B. Humphrey, TREM2- and DAP12-dependent activation of PI3K requires DAP10 and is inhibited by SHIP1, Sci. Signal. 3 (122) (2010) ra38.
[27] L. Zhong, Z. Wang, D. Wang, Z. Wang, Y.A. Martens, L. Wu, et al., Amyloid-beta modulates microglial responses by binding to the triggering receptor expressed on myeloid cells 2 (TREM2), Mol. Neurodegener. 13 (1) (2018) 15.
[28] B. Kalyanaraman, V. Darley-Usmar, K.J. Davies, et al., Measuring reactive oxygen and nitrogen species with fluorescent probes: challenges and limitations, Free Radic. Biol. Med. 52 (1) (2012) 1–6.
[29] T. Kiyoshima, N. Enoki, I. Kobayashi, T. Sakai, K. Nagata, H. Wada, et al., Oxidative stress caused by a low concentration of hydrogen peroxide induces senescence-like changes in mouse gingival fibroblasts, Int. J. Mol. Med. 30 (5) (2012) 1007–1012.
[30] M. Shimoe, T. Yamamoto, N. Shiomi, K. Tomikawa, S. Hongo, K. Yamashiro, et al., Overexpression of Smad2 inhibits proliferation of gingival epithelial cells, J. Periodontal. Res. 49 (3) (2014) 290–298.
[31] D. Lian, L. Dai, Z. Xie, X. Zhou, X. Liu, Y. Zhang, et al., Periodontal ligament fibroblasts migration injury via ROS/TXNIP/Nlrp3 inflammasome pathway with

Porphyromonas gingivalis lipopolysaccharide, Mol. Immunol. 103 (2018) 209–219.
[32] T.B. Bedran, M.P. Mayer, D.P. Spolidorio, D. Grenier, Synergistic anti-inflammatory activity of the antimicrobial peptides human beta-defensin-3 (hBD-3) and cathelicidin (LL-37) in a three-dimensional co-culture model of gingival epithelial cells and fibroblasts, PloS One 9 (9) (2014), e106766.
[33] D. Kim, B. Langmead, S.L. Salzberg, HISAT: a fast spliced aligner with low memory requirements, Nat. Methods 12 (4) (2015) 357–360.
[34] A. Subramanian, P. Tamayo, V.K. Mootha, S. Mukherjee, B.L. Ebert, M.A. Gillette, et al., Gene set enrichment analysis: a knowledge-based approach for interpreting genome-wide expression profiles, Proc. Natl. Acad. Sci. U. S. A 102 (43) (2005) 15545–15550.
[35] V.K. Mootha, C.M. Lindgren, K.F. Eriksson, A. Subramanian, S. Sihag, J. Lehar, et al., PGC-1alpha-responsive genes involved in oxidative phosphorylation are coordinately downregulated in human diabetes, Nat. Genet. 34 (3) (2003) 267–273.
[36] Y. Sun, Y. Weng, C. Zhang, Y. Liu, C. Kang, Z. Liu, et al., Glycosylation of dentin matrix protein 1 is critical for osteogenesis, Sci. Rep. 5 (2015) 17518.
[37] Y. Weng, Y. Liu, H. Du, L. Li, B. Jing, Q. Zhang, et al., Glycosylation of DMP1 is essential for chondrogenesis of condylar cartilage, J. Dent. Res. 96 (13) (2017) 1535–1545.
[38] T. Miyazaki, Z. Zhao, Y. Ichihara, D. Yoshino, T. Imamura, K. Sawada, et al., Mechanical regulation of bone homeostasis through p130Cas-mediated alleviation of NF-κB activity, Sci. Adv. 5 (9) (2019), eaau7802.